The *bop2-1* Mutation Reveals Radial Asymmetry in the Inner Dynein Arm Region of *Chlamydomonas reinhardtii*

Stephen J. King, William B. Inwood, Eileen T. O'Toole, Joy Power, and Susan K. Dutcher

Department of Molecular, Cellular, and Developmental Biology, University of Colorado, Boulder, Colorado 80309-0347

Abstract. Strains of *Chlamydomonas reinhardtii* with a mutant allele at the *BOP2* locus swim slowly and have an abnormal flagellar waveform similar to previously identified strains with defects in the inner arm region. Double mutant strains with the *bop2-1* allele and any of 17 different mutations that affect the dynein arm region swim more slowly than either parent, which suggests that the *bop2-1* mutation does not affect solely the outer dynein arms, the I1 or *ida4* inner dynein arms, or the dynein regulatory complex. Flagellar axonemes isolated from *bop2-1* cells are missing a phosphorylated polypeptide of 152 kD. Electron microscopic analysis shows that *bop2-1* axonemes are missing density in the inner dynein arm region. Surprisingly, two populations of images were observed in longitudinal sections of axonemes from the *bop2-1* strain. In the 10 longitudinal axonemes examined, a portion of the dynein regulatory complex and a newly identified structure, the projection, are affected. In five of these 10 longitudinal axonemes examined, two lobes of the *ida4* inner arm are also missing. By examining the cross-sectional images of wild-type and *bop2-1* axonemes at each outer doublet position around the axoneme, we have determined that the *bop2-1* mutation affects the assembly of inner arm region components in a doublet specific manner. Doublets 5, 6, and 8 have the most severe deficiency, doublet 9 has an intermediate phenotype, and doublets 2, 3, 4, and 7 have the least severe phenotype. The *bop2-1* mutation provides the first evidence of radial asymmetry in the inner dynein arm region.

In the unicellular green alga *Chlamydomonas reinhardtii*, two flagella generate force to move the cell. The beat stroke is highly asymmetric and consists of two stages. In the effective stage, a power stroke, which travels almost entirely in two dimensions, is initiated by a single bend that forms near the base of the flagellum while the remainder of the flagellum is straight. In the recovery stage, a three-dimensional stroke is initiated near the base of the flagellum and propagates distally, leaving the flagellum in the starting position (Brokaw et al., 1982). An asymmetric beat stroke suggests that the flagella are structurally asymmetric. The focus of much research in recent years has been the regulation of dynein activity, but the relationship between asymmetry of the beat stroke and dynein regulation is not well understood.

Three types of asymmetry have been observed in the flagella of *C. reinhardtii*. Asymmetries have been reported among specific outer doublets of the flagella (radial asymmetry), along the length of the flagella (proximal/distal asymmetry), and between the two flagella (*cis/trans* asymmetry). For example, outer doublets 1, 5, and 6 are different from the other outer doublets. Doublets 1, 5, and 6 contain a B-tubule projection, which extends partially across the lumen of the microtubule (Hoops and Witman, 1983). These three doublets are located in the plane of the power stroke; doublets in these positions are predicted to exhibit the least microtubule sliding relative to their neighbors during the power stroke (Hoops and Witman, 1983). Several mutant strains (*mbol,2,3*), which are missing the B-tubule projections from doublets 5 and 6, are able to swim only backwards and the flagella utilize a sinusoidal waveform that is similar to sperm flagella waveforms (Segal et al., 1984). A two-membered cross-bridge that extends from doublet 1 towards doublet 2 and the absence of an outer dynein arm from over 90% of the length of doublet 1 are two additional radial asymmetries (Hoops and Witman, 1983).

The second flagellar asymmetry exists between regions that are proximal to the basal bodies and regions that are distal. Several of the high molecular weight (HMW)[1] inner arm dynein chains are hypothesized to be localized to specific regions of the flagella. Electron microscopic and biochemical examinations of partially extracted axonemes suggest that HMW polypeptide 3′ is present in proximal but not in distal portions and the HMW polypeptide 2 is localized predominantly to proximal regions of the axoneme

Address all correspondence to S. K. Dutcher, Department of Molecular, Cellular, and Developmental Biology, University of Colorado, Boulder, CO 80309-0347. Phone: (303) 492-6342. Fax: (303) 492-7744.

1. *Abbreviations used in this paper*: drc, dynein regulatory complex; HMW, high molecular weight.

(Piperno and Ramanis, 1991). A second example of proximal/distal asymmetry is the sensitivity of flagella to the addition of colchicine. When colchicine is added to the medium, the distal 25–50% of the flagella is disassembled. The biochemical basis for this sensitivity is not known (Dentler and Adams, 1992), but it is possible that some factors that affect flagellar length may be asymmetrically positioned along the length of the axoneme. A third example of proximal/distal asymmetry is the localization of the B-tubule projections and two-membered cross-bridge described above. The B-tubule projections are present only in the proximal 40–57% of the flagella and the two-membered cross-bridge is present only in the proximal one quarter of the axoneme (Hoops and Witman, 1983).

The final observed asymmetry is based on functional differences between the two flagella. The two flagella are termed *cis* and *trans* based on their position relative to an eyespot; the *cis* flagellum is closer to the eyespot (Huang et al., 1982*a*). The *trans* flagellum is always initiated from the parental basal body while the *cis* flagellum is initiated from the daughter basal body (Holmes and Dutcher, 1989). *Cis/trans* asymmetries may play a role in phototactic behavior. Supporting this hypothesis, different responses between the two flagella to light (Rüffer and Nultsch, 1991) and Ca^{2+} (Kamiya and Witman, 1984) stimuli have been observed. The beat patterns of the two flagella are altered coordinately to changes in light stimuli. The beat amplitude of one flagellum is increased while the beat amplitude of the other flagellum is decreased in response to changes in light intensity in vivo (Rüffer and Nultsch, 1991). Preferential beating of the two axonemes is observed in response to different Ca^{2+} concentrations in detergent-extracted cell models. The *cis* axoneme is more active at 10^{-9} M Ca^{2+} whereas the *trans* axoneme is more active at 10^{-7} M Ca^{2+} (Kamiya and Witman, 1984). No biochemical or morphological difference between the two flagella has been reported.

We have characterized a mutation in *C. reinhardtii* that is involved in the control of flagellar waveform (Dutcher et al., 1988). The *bop2-1* strain was isolated as an extragenic suppressor of the motility phenotype observed in a *pf10* strain (*bop* = bypass of paralysis). The *bop2-1* strain exhibits a swimming phenotype that is similar to those of inner dynein arm region mutant strains. Flagellar axonemes from the *bop2-1* strain are missing a 152-kD phosphoprotein that was not localized previously to a particular axonemal structure. Electron micrograph analyses of *bop2-1* axonemes demonstrate that this mutation affects the assembly of inner arm region components in a doublet specific manner. The *bop2-1* mutation provides the first evidence of radial asymmetry in the inner dynein arm region of the flagella.

Materials and Methods

Microscopic Techniques

Slides were prepared and phase microscopy was performed as described previously (Inwood, 1985). The swimming patterns of cells and flagellar movements were observed and recorded on a Zeiss Universal microscope using darkfield optics with a 16× or 40× Plan objective and an oil darkfield condenser (NA = 1.2–1.4). Samples were illuminated by a xenon lamp powered by a Chadwich Helmuth model 136 power supply. The power supply, kindly supplied by E. D. Salmon (University of North Carolina, Chapel Hill, NC), was pulsed by a Grass Instruments pulse generator for stroboscopic effects. Images were recorded with a 35 mm Nikon camera on Tri-X film.

Gel Electrophoresis

Two-dimensional SDS-PAGE was performed as previously described (Piperno et al., 1981). In the ^{32}P analysis of wild-type and *bop2-1* axonemes, cells were harvested from low-phosphate medium plates into nitrogen-free, phosphate-free medium and then incubated for 10 min with [^{32}P]orthophosphoric acid at a ratio of 1 mCi/10^9 cells (Segal et al., 1984). Over 90% of the radiolabel was taken up by the cells. One-dimensional Neville gels with a 4–8% acrylamide gradient were prepared as in Adams et al. (1981). Autoradiography was performed as described by Segal et al. (1984). Gels were silver stained by the method of Blum et al. (1987) or the method of Merrill et al. (1981) with the following modifications. Gels were washed three times for 30 s each after potassium dichromate treatment; they were left for 45 min in bright light in the silver nitrate solution; and a wash with sodium carbonate preceded the wash with sodium carbonate and formaldehyde. After staining, these gels were photographed in a 2% glycerol solution with a Wratten No. 8 filter and then dried onto a dialysis membrane. Molecular weights were calculated from the MW-SDS-200 standards from Sigma Chemical Co. (St. Louis, MO).

Dikaryon Rescue Experiments

Temporary dikaryons were constructed as described in Dutcher et al. (1984). For the biochemical analysis of the dikaryons, a wild-type parent was grown on solid medium with a reduced concentration of sulfate and the second parent (*bop2 pf10*) was grown on similar medium containing 25 mCi of [^{35}S]sulfuric acid/liter for 3 d at 25°C in constant light (25 $\mu E/m^2/s$) and then for 2 d at 21°C in subdued light (8 $\mu E/m^2/s$). Cells of each strain were harvested into nitrogen-free medium at a density of $\sim 1 \times 10^7$ cells/ml and allowed to differentiate for 5 to 18 h. The gametes of opposite mating types were mixed. After 10 min, anisomycin was added to 60 μM to inhibit protein synthesis. (Anisomycin was a gift of Pfizer, Inc., Groton, CT). After 1 h, flagellar axonemes were isolated as described previously (Porter et al., 1992). Because only 30% of the cells mated in the experiment, overexposures of the autoradiograms were examined.

Reversion Analysis

A *bop2-1 oda9 enh2* parental strain was mutagenized by ultraviolet irradiation to 80% survival (Dutcher et al., 1988). *oda9* is a mutation that affects the assembly of the entire outer dynein arm (Kamiya, 1988) and *enh2* is a mutation found in our stock collection that enhances the phenotype of the *bop2-1 oda9* double mutant strain. *bop2-1 oda9* strains swim slower than either parental strain and *enh2* has no phenotype alone or with *bop2-1* or *oda9*, singly. Enrichment screens for swimming cells were performed by transferring 10% of the medium near the meniscus to new medium. Once transferred, the cells were allowed to grow to $\sim 1 \times 10^6$ cells/ml and the procedure was repeated. After four rounds of enrichment, cells were plated for single colonies and the swimming phenotypes were analyzed. To identify intragenic reversion events at one of the three loci, the strains were crossed by a wild-type strain. Between 6 and 18 tetrads were analyzed for each strain with an average of 13.7 tetrads. Intragenic revertants or extragenic suppressors that are closely linked to *bop2-1*, *oda9*, or *enh2* should produce tetrads with four meiotic progeny that swim and no meiotic progeny that fail to swim. The revertants that produced all swimming progeny were crossed to three additional strains (*bop2-1*, *oda9*, and *oda9 enh2*) and the meiotic progeny were analyzed to determine the locus where reversion may have occurred. Intragenic revertants at the *BOP2* locus (or closely linked extragenic suppressors) would produce meiotic progeny that cannot swim only when crossed to the *bop2-1* tester, which could generate *bop2-1 oda9 enh2* progeny. Events at or near the *ODA9* locus would give rise to nonswimmers when crossed to either the *oda9* or *oda9 enh2* tester, and events at or near the *ENH2* locus would give rise to nonswimmers only when crossed to the *oda9 enh2* tester.

Electron Microscopy, Digitization, and Averaging Techniques

Axonemes were prepared for electron microscopy as described in Porter et al. (1992). Sections of 60-nm nominal thickness were used for the cross-sectional analysis; 40-nm sections were used for the longitudinal analysis. All microscopy was performed on a Philips CM10 electron microscope (Philips Electronic Instruments Co., Mahwah, NJ) operating at 80 kV. The methods for selecting, digitizing, averaging, normalizing, and comparing cross-sectional outer doublets were as described previously (Mastronarde et al., 1992). Sample averages were obtained from 50 to 100 outer doublets

selected from each preparation. To control for preparation variability, averages from at least five different preparations of the same strain were normalized on the optical density of the outer dynein arms and combined to obtain a grand average (Mastronarde et al., 1992).

To obtain cross-sectional average images for any particular doublet, we identified and grouped corresponding microtubule doublets from the nine positions around the axoneme. Doublet 1 was identified by the absence of an outer dynein arm. In images where we could see B-tubule projections, the doublet identified as doublet 1 by the absence of the outer dynein arm always correlated with doublet 1 as identified by the location of the B-tubule projections. A computer program written by Dr. David Mastronarde (Boulder Laboratory for 3-D Fine Structure, Boulder, CO) was then used to identify and average doublets from the other eight positions. Individual outer doublet averages and group outer doublet averages, which are comprised of any subset of individual outer doublet averages, were then compared in an analysis of variance as described below. Images of doublet 1 could not be normalized on the density of their outer dynein arms since this structure is missing. Images of doublet 1 were therefore normalized on the basis of individual microtubule protofilaments (Mastronarde et al., 1992). 12% of axonemal cross-sections did not have a clear doublet 1 and these images were not included in the analysis of radial asymmetry.

The techniques used for digitizing and averaging the longitudinal images and the methods for comparing images were as described in Mastronarde et al. (1992). We selected images of axonemes with clear outer arms, radial spokes, and five or more of the 96-nm inner arm region repeating units. The selected repeating units from each longitudinal image were aligned and averaged to provide an individual axoneme average. Either a subset or all of the individual axoneme averages from a particular strain were then aligned and averaged together to give a longitudinal group or grand average, respectively.

Quantitative comparisons between wild-type and *bop2-1* averages were performed for both cross-sectional and longitudinal images. Difference images were obtained from a pixel-by-pixel nested analysis of variance (Mastronarde et al., 1992). For the cross-sectional difference images, differences not significant at the 0.05 level were set to zero. For the longitudinal difference images, differences not significant at the 0.0025 level were set to zero. During the course of our work, it came to our attention that the longitudinal model published in Mastronarde et al. (1992) was a vertical mirror image of the correct orientation of inner arm region structures. The dynein arm structures in the figures of Mastronarde et al. (1992) should be interpreted as protruding through the back of the microtubule instead of extending toward the viewer as was originally presented. The longitudinal images and models in this paper are correctly orientated with the proximal regions of the 96-nm repeats to the left and the dynein arm structures extending toward the viewer.

Other Methods

The media for culturing cells were as described previously (Holmes and Dutcher, 1989). Many of the mutant strains were kindly provided by Dr. Elizabeth Harris of the Chlamydomonas Genetics Center (Duke University, Durham, NC). The *ida1* and *ida4* strains were provided by Dr. Ritsu Kamiya (University of Tokyo, Tokyo, Japan). The wild-type strain used throughout this work was strain 137c (CC-125). Genetic analysis was performed essentially as described by Levine and Ebersold (1960) and Harris (1989).

Results

Phenotypic Analysis

The *bop2-1* mutation was isolated as an extragenic suppressor that restored partial motility to the *pf10* mutant strain (Dutcher et al., 1988). *pf10* mutant cells have an altered flagellar waveform; the beat stroke is nearly symmetric and the cells are unable to move forward (Inwood, 1985). In the *pf10 bop2-1* double mutant strain, the cells swim with a velocity of 88 ± 15 μm/s (n = 50 cells) compared to a velocity of 176 ± 7 μm/s (n = 50 cells) for wild-type cells. *bop2-1* cells swim with a velocity of 102 ± 10 μm/s (n = 50 cells) and exhibit a flagellar waveform that resembles the pattern observed in previously characterized inner arm region mutant strains (Brokaw and Kamiya, 1987; Kamiya, 1988; Porter et al., 1992). The *BOP2* locus maps to a previously unidentified locus on linkage group IV (Dutcher et al., 1988).

Genetic Interactions of the bop2-1 Mutation

We performed epistasis tests with *bop2-1* and other flagellar mutations. Since the *bop2-1* strain had a motility phenotype similar to other dynein region mutant strains, double mutant strains were constructed with four classes of dynein region mutant strains. We examined representative alleles at each of 10 loci that fail to assemble outer dynein arms, alleles at three loci that fail to assemble a complete dynein regulatory complex (drc), alleles at one locus that fail to assemble the I1 inner dynein arms, and one allele that fails to assemble the inner dynein arms affected by the *ida4* mutation. In all cases, the double mutant strains have a new phenotype. The double mutant strains have a reduced velocity compared with either parental strain (Table I). Therefore the *bop2-1* mutation is unlikely to affect solely that I1 or *ida4* inner dynein arms, the outer dynein arms, or the drc. Many of the double mutant strains showed increased percentages of aflagellate cells in the population (data not shown). A similar aflagellate phenotype has been observed previously in many double mutant strains and is not specific to combinations of mutations in the dynein arms (Piperno et al., 1990; Porter et al., 1992).

We also asked if the *bop2-1* mutation was a bypass suppressor of several paralyzed flagellar mutations. Some classes of mutant strains are able to suppress the paralysis that results from mutations that disrupt radial spoke and/or central pair assembly (Huang et al., 1982*b*; Piperno et al., 1992; Porter et al., 1992). 10 mutations that affect structures or processes that are required for normal flagellar beating

Table I. Genetic Interactions between bop2-1 and Other Dynein Arm Mutations

Mutant strain	Structure/ polypeptide affected	Single mutant phenotype	Double mutant phenotype
bop2-1	–	Slow swimming	Slower swimming
oda1	ODA	Slow swimming	Slower swimming
oda2	ODA	Slow swimming	Slower swimming
oda3	ODA	Slow swimming	Slower swimming
oda4	ODA	Slow swimming	Slower swimming
oda5	ODA	Slow swimming	Slower swimming
oda6	ODA	Slow swimming	Slower swimming
oda7	ODA	Slow swimming	Slower swimming
oda8	ODA	Slow swimming	Slower swimming
oda9	ODA	Slow swimming	Slower swimming
oda10	ODA	Slow swimming	Slower swimming
$sup_{pf}1$	ODA	Slow swimming	Slower swimming
pf2	DRC	Slow swimming	Slower swimming
pf3	DRC	Slow swimming	Slower swimming
$sup_{pf}3$	DRC	Wild-type motility	Slow swimming
pf9-1, pf9-2	IDA	Slow swimming	Slower swimming
ida1	IDA	Slow swimming	Slower swimming
ida4	IDA	Slow swimming	Slower swimming

Structure/polypeptide affected compiled with data from McVittie, 1972, Huang et al., 1982*b*, Kamiya, 1988, Kamiya et al., 1991, and Porter et al., 1992. *ODA*, outer dynein arms; *DRC*, dynein regulatory complex; *IDA*, inner dynein arms.

Table II. Genetic Interactions between bop2-1 and Paralyzed Flagellar Mutations

Mutant strain	Structure/ polypeptide affected	Single mutant phenotype	Double mutant phenotype
pf18	CP	Paralyzed, rigid	Very short flagella, paralyzed
pf20	CP	Twitching	No effect, twitching
pf6	CPP	Twitching	No effect, twitching
pf1	RS	Twitching	No effect, twitching
pf14	RS	Paralyzed	No effect, paralyzed
pf27	RS	Twitching	No effect, twitching
pf5	RS, IDA	Paralyzed	No effect, paralyzed
pf23	IDA	Paralyzed	No effect, paralyzed
pf22	ODA, IDA	Paralyzed	No effect, paralyzed
pf12	ND	Twitching	No effect, twitching

Structure/polypeptide affected compiled with data from McVittie, 1972; Luck et al., 1977; Huang et al., 1979; Adams et al., 1981; Huang et al., 1981; Dutcher et al., 1984; and Luck and Piperno, 1989.
CP, central pair; *CPP*, central pair projections; *RS*, radial spokes; *IDA*, inner dynein arms; *ODA*, outer dynein arms, *ND*, not determined.

were tested (Table II). In all cases, the double mutant strains were paralyzed, so the *bop2-1* mutation does not act as a bypass suppressor of the mutations tested.

Biochemical Phenotype of bop2-1 Axonemes

We examined *bop2-1* axonemes by two-dimensional SDS-PAGE to determine if a biochemical phenotype existed. Both wild-type and *bop2-1* cells were labeled with [^{35}S]sulfuric acid and flagellar axonemes were isolated. A single prominent polypeptide present in wild-type axonemes is missing from *bop2-1* axonemes (Fig. 1). This polypeptide has a molecular weight of 152 kD and an isoelectric point of 6.2 and is not missing in any previously characterized mutant strain.

We examined axonemes from the progeny of tetrads from a *bop2-1* × wild-type cross that had been incubated with [^{32}P]orthophosphoric acid to ask if the 152-kD polypeptide is present in axonemes in a phosphorylated form. The axonemes were analyzed by one-dimensional PAGE. A 152-kD polypeptide was present in wild-type segregants and absent in *bop2-1* segregants (Fig. 2). It is likely that the 152-kD polypeptide is present only in a phosphorylated form in the axoneme since only one spot is observed by ^{35}S two-dimensional SDS-PAGE of wild-type axonemal polypeptides in this region (Fig. 1). Therefore, the *bop2-1* mutation results in the loss of a single 152-kD phosphoprotein from the axoneme.

Cosegregation of the biochemical and flagellar phenotypes was assayed in meiotic progeny from a *bop2-1 pf10* × wild-type cross. When analyzed by one-dimensional PAGE, the 152-kD polypeptide was missing from eighteen independent meiotic progeny that exhibited the *bop2-1* motility phenotype and each of these strains was able to suppress the *pf10* mutation in an additional cross (data not shown). Therefore, the motility, suppression, and biochemical phenotypes cosegregate with the *bop2-1* mutation and are at most 5.3 centimorgans apart.

Biochemical Phenotype of Double Mutant Strains

We examined the biochemical phenotype of several double

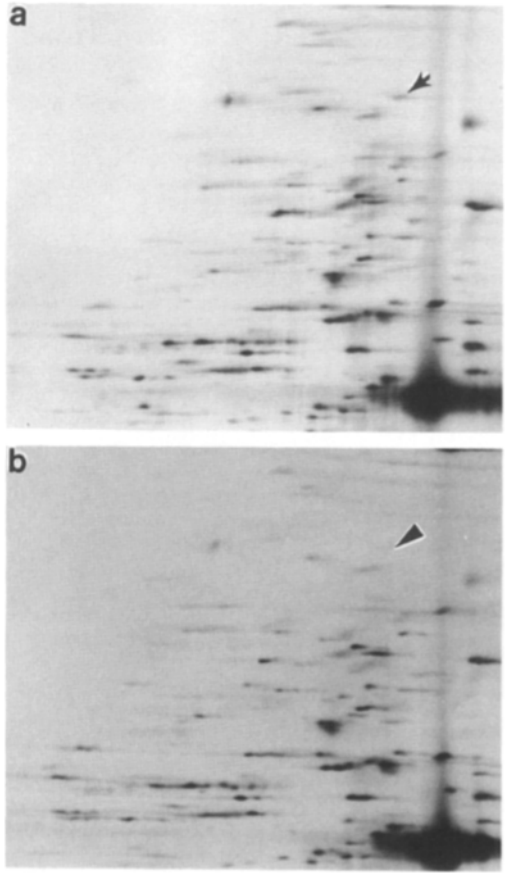

Figure 1. Autoradiogram of [^{35}S]sulfuric acid labeled axonemal polypeptides resolved by two-dimensional gel electrophoresis. (*a*) Polypeptides from wild-type axonemes. (*b*) Polypeptides from *bop2-1* axonemes. Portions of the gel from apparent molecular weights of 200,000 to 50,000 are shown. Acidic polypeptides are on the right side of the figure. The arrow indicates a 152-kD polypeptide with an isoelectric point of 6.2 that is present in wild-type axonemes but missing in *bop2-1* axonemes. The arrowhead indicates the expected position of the 152-kD polypeptide. The intensity of several polypeptides is variable. An examination of autoradiograms from over 30 independent axonemal preparations from wild-type and various other mutant strains showed that this variability is not linked to the *BOP2* locus.

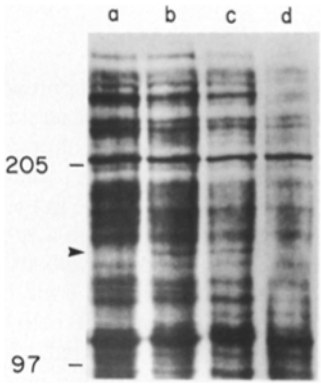

Figure 2. Autoradiogram of [^{32}P]orthophosphoric acid labeled axonemal polypeptides resolved by one-dimensional gel electrophoresis. Axonemal polypeptides from the progeny of a tetrad derived from a cross of *bop2-1* by *BOP2* parents were examined. Zoospores a and d have the *bop2-1* mutation and are missing a 152-kD phosphoprotein. Portions of the gel from apparent molecular weights of 300,000 to 95,000 are shown. The arrow indicates the polypeptide missing from *bop2-1* axonemes.

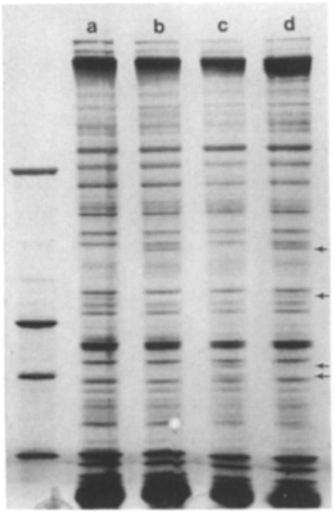

Figure 3. Silver stained one-dimensional gel electrophoretograms of a meiotic tetrad from a cross of *pf9-2 BOP2* × *PF9 bop2-1* parents. Molecular weight standards of 205, 116, 97, and 66 kD are shown on the left. Arrows indicate the missing polypeptides with apparent molecular weights of 152,000, 140,000, and the additional polypeptides with apparent molecular weights of 100,000, and 97,000. (*a*) Axonemal polypeptides from *bop2-1 PF9* cells. A polypeptide of 152 kD is missing. (*b*) Axonemal polypeptides from *BOP2 pf9-2* cells. A polypeptide of 140 kD is missing. This gel system does not resolve the 110-kD polypeptide missing from *pf9* axonemes. (*c*) Axonemal polypeptides from *bop2-1 pf9-2* cells. The 152- and 140-kD polypeptides are missing as in lanes *a* and *b*. In addition, axonemes from the double mutant strain contain two new additional polypeptides with apparent molecular weights of 100,000 and 97,000. (*d*) Axonemal polypeptides from wild-type (*BOP2 PF9*) cells.

mutant strains. Axonemes from inner arm region double mutant strains were analyzed by one-dimensional PAGE followed by silver staining. Axonemes from the *bop2-1 pf9* double mutant strain are missing the 152-kD polypeptide associated with the *bop2-1* mutation, plus two HMW dynein chains (data not shown) and two intermediate chains of 140 and 110 kD that are associated with the *pf9* defect. Surprisingly, two additional polypeptides are present in *bop2-1 pf9* axonemes that are not present in axonemes from wild-type or either of the single mutant strains (Fig. 3). These new polypeptides have apparent molecular weights of 100,000 and 97,000. The extra polypeptides were present in axonemes from ten independent meiotic progeny with three different *pf9* alleles (*pf9-1*, *pf9-2*, and *ida1-98*). Axonemes from *bop2-1 ida4* and *bop2-1 pf3* strains do not have any additional polypeptides and only the 152-kD polypeptide and the polypeptides normally deficient in the *ida4* or *pf3* axonemes are missing (data not shown). It is interesting that axonemes from the drc mutant strain, $sup_{pf}3$, also contain two novel polypeptides (~50 and 58 kD) and that no other mutations show a stable incorporation of novel polypeptides in the axoneme. No evidence for a role of proteolysis has been presented in the assembly or regulation of flagellar function.

Dikaryon Rescue Analysis

Dikaryon rescue experiments in *Chlamydomonas* have provided evidence about gene–gene product relationships (Luck et al., 1977; Dutcher et al., 1984). An analysis of temporary dikaryons was used to examine the relationship between the suppression of the pf10 motility phenotype and the 152-kD polypeptide. Dikaryons were examined from three different matings, *BOP2 pf10* × *BOP2 PF10*, *bop2-1 pf10* × *BOP2 PF10*, and *bop2-1 pf10* × *BOP2 pf10* (Table III). Examination of the flagellar beat strokes in quadriflagellate zygotic cells from the *BOP2 pf10* × *BOP2 PF10* mating showed that *pf10* and wild-type flagella maintain different beat strokes in temporary dikaryons, as previously observed (Dutcher, 1986). However, in *bop2-1 pf10* × *BOP2 PF10* and *bop2-1 pf10* × *BOP2 pf10* dikaryons, the suppression of the pf10 phenotype by the *bop2-1* mutation is lost within one hour in two of the four flagella. Presumably, the wild-type BOP2 gene product is present in the cytoplasm of the *BOP2* parent, and incorporation into the flagella results in the loss of suppression. Therefore the *bop2-1* allele is recessive to the wild-type allele in dikaryons as well as in heterozygous diploid strains (Dutcher et al., 1988).

To determine if the 152-kD polypeptide is present in the *bop2-1 pf10* cytoplasmic pool of axonemal proteins, we mated ^{35}S-labeled *bop2-1 pf10* cells with unlabeled *BOP2 PF10* cells and isolated the axonemes from the heterozygous dikaryons one hour after mating. The recovery of the pf10 phenotype in dikaryons is not accompanied by the appearance of a labeled 152-kD protein on one-dimensional gels (data not shown). This result implies that the 152-kD phosphoprotein is not available from the cellular pool of labeled polypeptides contributed by the *bop2-1 pf10* cells.

Reversion Analysis

We performed a reversion analysis of the *bop2-1* allele with the goal of identifying the gene product of this locus. We hoped to find pseudorevertants that would have an altered biochemical phenotype compared to both the wild-type and original mutant strains (Luck et al., 1977). Since revertants of the *bop2-1* slow swimming phenotype would be difficult to identify without a laborious microscopic screen, we mutagenized a mutant strain that had a synthetic phenotype. The triple mutant strain that contains *bop2-1*, the outer dynein arm mutation *oda9*, and a third mutation *enh2*, has very few motile cells in the supernatant when grown in the presence of 25 $\mu E/m^2/s$ of white light and forms a pellet that contains primarily aflagellate cells. We screened for new mutational events that restored motility to this triple mutant strain as as-

Table III. Heterozygous Dikaryon Phenotypes

Parental genotypes	Motility phenotype of dikaryon flagella directly after mating	Motility phenotype of dikaryon flagella 1 h after mating
BOP2 pf10 × *BOP2 PF10*	2 wild-type 2 pf10	2 wild-type 2 pf10
bop2-1 pf10 × *BOP2 PF10*	2 wild-type 2 suppressed	2 wild-type 2 pf10
bop2-1 pf10 × *BOP2 pf10*	2 pf10 2 suppressed	4 pf10

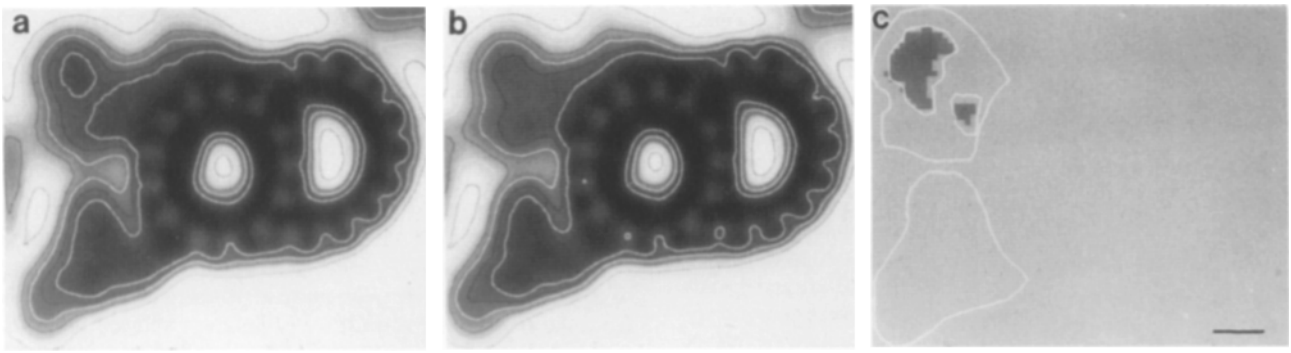

Figure 4. Cross-sectional structural phenotype of *bop2-1* axonemes. Inner dynein arm region structure is in the top left of each panel; outer dynein arm structure is in the bottom left of each panel. The contour lines represented in *a* and *b* have the same density scale. The outlines in *c* are not density contours; they have been drawn by hand to facilitate comparing the location of structural defects in different figures. (*a*) The grand average from five independent preparations of wild-type axonemes comprising a total of 268 doublets. (*b*) The grand average from six independent preparations of *bop2-1* axonemes comprising a total of 301 doublets. (*c*) A difference image between wild-type and *bop2-1* grand averages with differences not significant at the 0.05 level of significance set to zero. Bar, 10 nm.

sayed by the presence of cells in the supernatant of liquid medium. 53 independent revertants were isolated and analyzed as described in Materials and Methods. 38 of the 53 revertants contained extragenic suppressors. One strain appeared to be an intragenic revertant at the *ENH2* locus. The remainder ($n = 14$) appeared to be intragenic revertants at the *ODA9* locus. Since no *bop2-1* revertants were found, the reversion analysis was unable to provide evidence about the gene product of the *BOP2* locus.

Structural Phenotype of the bop2-1 Strain

Axonemes from *bop2-1* cells were examined by electron microscopy to see if they displayed a structural phenotype. Because the motility phenotype of the *bop2-1* strain is similar to that of previously characterized inner arm region mutant strains, we focused our analysis on this region. Axonemes from wild-type and *bop2-1* strains were examined as described in Materials and Methods. The grand averages of cross-sectional images from these strains are shown in Fig. 4 (*a* and *b*). From a comparison of the contour lines in the inner arm region in Fig. 4 (*a* and *b*), a loss of density is apparent in the *bop2-1* grand average compared to the wild-type grand average. A difference image between the wild-type and *bop2-1* grand averages shows that two lobes of density are missing in *bop2-1* axonemes compared to wild-type axonemes (Fig. 4 *c*). The more severe loss falls in the inner domain of the inner arm region and an additional loss is located near the base of the inner arm region. The *bop2-1* structural phenotype is statistically different from the phenotypes of axonemes from the *pf23, pf9, ida4,* or *pf2* mutant strains, which also have defects in the inner arm region (data not shown; Mastronarde et al., 1992). Therefore, the *bop2-1* allele represents a new class of mutation that affects the structure of the inner arm region.

We performed a longitudinal analysis of axonemes from the *bop2-1* strain to ask which of the major lobes of density within each 96-nm repeating unit of the inner arm region were affected. The grand averages from wild-type and *bop2-1* longitudinal images are shown in Fig. 5 (*a* and *b*), respectively. A different image between the wild-type and *bop2-1* grand averages shows that the *bop2-1* axonemes are deficient in four structures (Fig. 5 *c*). Structure 1 (hereafter called the projection) extends distally between lobe 4 (described below) and the outer domain of the inner arm region, is lightly stained, and was not identified previously (Mastronarde et al., 1992). Structure 2 is a portion of the drc and was missing in *pf2* axonemes. Structure 3 is a portion of the most distally located *ida4* structure in the 96-nm repeat (Mastronarde et al., 1992). Structure 4 is located under the proximal radial spoke; it was missing in *ida4* axonemes and was termed lobe 4 (Mastronarde et al., 1992). As might be expected from the cross-sectional phenotype, the longitudinal phenotype of the *bop2-1* strain is significantly different from the phenotypes of the *pf23, pf9, ida4,* or *pf2* mutant strains (data not shown; Mastronarde et al., 1992). Thus, the *bop2-1* mutation affects the assembly of one newly identified structure and three previously characterized structures.

A conspicuous feature of the individual longitudinal averages obtained from *bop2-1* axonemes was the heterogeneity of the phenotypes. Of the 10 *bop2-1* individual axoneme averages, five were missing the lobe 4 density and five contained the lobe 4 density. The lobe 4 density was present in all nine wild-type individual axoneme averages. In the *bop2-1* axonemes whose individual averages were missing lobe 4 density, the density was missing in all of the repeats. In the axonemes whose individual averages contained lobe 4 density, the density was present in all of the 96-nm repeats (data not shown). One individual axoneme average from *bop2-1* axonemes that is deficient for lobe 4 is shown in Fig. 5 *d* and two individual axoneme averages that contain lobe 4 are shown in Fig. 5 (*e* and *f*).

Because of the heterogeneity in individual axoneme averages, we averaged the *bop2-1* axonemes that contained or lacked the lobe 4 density to define the fine structure of both classes of axonemes. The group average of the five axonemes that contained the lobe 4 density and a difference image compared to wild-type are shown in Fig. 5 (*g* and *h*). There was no significant difference from wild-type structure in either lobe 4 or the distally located *ida4* density. The group average of the five axonemes that lack lobe 4 density and a difference image compared to wild-type are shown in Fig. 5 (*i* and *j*). In this subset, in addition to lobe 4, the more distally located *ida4* structure is also deficient. Both sets of *bop2-1* axonemes

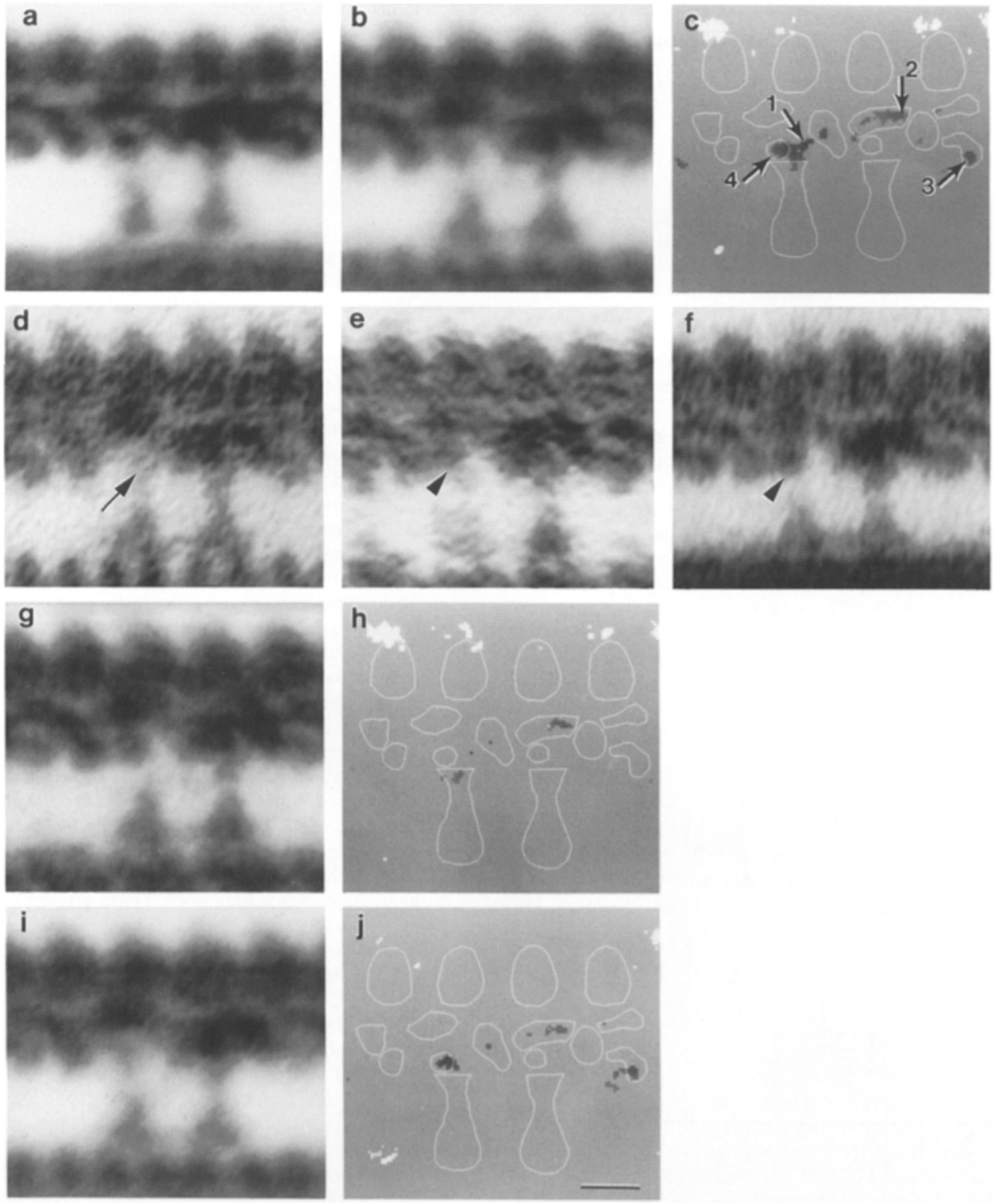

Figure 5. Longitudinal phenotypes of *bop2-1* axonemes. Outer dynein arms are at the top; radial spokes are at the bottom; the proximal end of the 96-nm repeating unit is at the left. Inner arm region structure is located between the radial spokes and outer dynein arms. (*a*) The grand average of wild-type from nine axonemes and 62 repeating units. (*b*) The grand average of *bop2-1* from 10 axonemes and 69 repeating units. (*c*) A difference image between wild-type and *bop2-1* grand averages. The structures labeled 1 through 4 are described in the text. (*d*) The individual axoneme average of a *bop2-1* axoneme that is missing the lobe 4 density (n = 6 repeating units). The arrow shows the expected position of lobe 4. (*e* and *f*) The individual axoneme averages of two *bop2-1* axonemes that contain the lobe 4 density (n = 6 and 7 repeating units, respectively). The arrowheads show the position of lobe 4. (*g*) The group average of five *bop2-1* axonemes that contain lobe 4 density (n = 32 repeating units). (*h*) A difference image between the wild-type grand average and the group average in *g*. (*i*) The group average of five *bop2-1* axonemes that are missing lobe 4 density (n = 37 repeating units). (*j*) A difference image between the wild-type grand average and the group average in *i*. In *c*, *h*, and *j*, differences not significant at the 0.0025 level of significance were set to zero. Bar, 25 nm.

are deficient for a portion of the drc and for the projection. Thus, the longitudinal grand average was a composite of axonemes missing a portion of the drc and the projection and axonemes missing those structures and two *ida4* inner arm structures.

Inner Arm Region Asymmetry Revealed by the bop2-1 Mutation

Two alternative models could explain the heterogeneity in the longitudinal images of *bop2-1* axonemes. First, the loss of structure in *bop2-1* axonemes could be a result of random loss of inner arm region structures. In this scenario, the deficiencies in the axonemes would not correlate to known flagellar asymmetries. In the second model, the loss of structure in *bop2-1* axonemes could be revealing one of the three inherent asymmetries in the axoneme; these are the radial, proximal/distal, and *cis/trans* asymmetries.

The longitudinal images do not contain sufficient positional information to determine if the heterogeneity correlates with one of the known asymmetries. However, cross-sectional images contain morphological markers for both radial and proximal/distal asymmetries. Therefore we reanalyzed the cross-sectional images to determine if a correlation existed between an axonemal asymmetry and the two classes of *bop2-1* axonemal defects. The relative position of each outer doublet in the data sets was determined based on its position relative to doublet 1, which lacks an outer dynein arm and contains a two-membered cross-bridge and a B-tubule projection (Hoops and Witman, 1983). Images from each specific outer doublet were pooled, aligned, averaged, and normalized to provide grand averages for each outer doublet position. A comparison of the integrated intensities of the whole inner arm region of doublets 2–9, individually and combined, from both *bop2-1* and wild-type axonemes is shown in Fig. 6. Our analysis shows that *bop2-1* outer doublets 5, 6, 8, and 9 contain significantly less inner arm region intensity than the corresponding wild-type doublets. *bop2-1* outer doublets 2, 3, 4, and 7 do not have significantly less intensity than the corresponding wild-type doublets even though the average intensity of these *bop2-1* outer doublets is less than the wild-type average (see below). Thus, it appears that the *bop2-1* mutation affects the assembly of inner arm region structures in a doublet specific manner. The *bop2-1* mutation provides the first evidence of radial asymmetry in inner arm region structures.

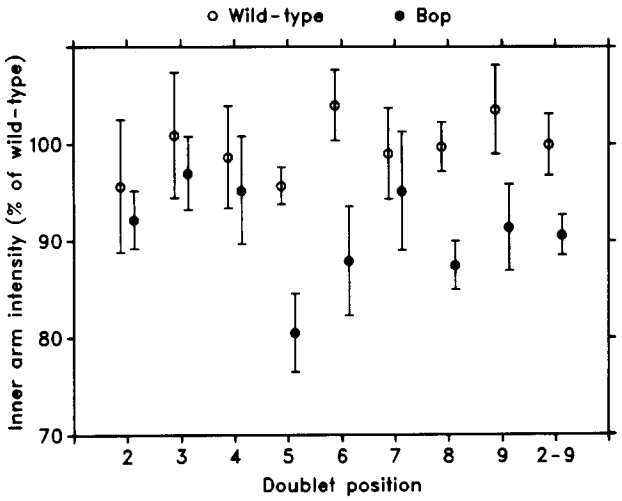

Figure 6. Integrated intensities of the whole inner arm region for wild-type and *bop2-1* axonemes at each outer doublet position. The integrated intensities are expressed as the percentage of the mean intensity for all wild-type doublets. Each data point presents the mean intensity at a position around the axoneme. The number of wild-type doublets averaged at positions 2 through 9 around the axoneme were 34, 37, 34, 28, 26, 28, 36, and 39, respectively. The number of *bop2-1* doublets averaged at positions 2 through 9 around the axoneme were 37, 44, 33, 33, 40, 36, 37, and 41, respectively. Error bars are 74% confidence limits. A nested analysis of variance of the whole inner arm was performed between wild-type and *bop2-1* at each doublet position; *bop2-1* doublets, 5, 6, 8, and 9 were found to be significantly different at the 0.05 level of significance. The integrated intensities of all wild-type (n = 268) and all *bop2-1* (n = 301) doublets are shown on the far right for comparison.

While the analysis above shows that inner arm region structure in outer doublets 5, 6, 8, and 9 is affected in *bop2-1* axonemes, we wanted to know if the affected doublets carried equivalent deficiencies. First, we compared the structure of wild-type doublets 5, 6, 8, and 9 to wild-type doublets 2, 3, 4, and 7. Except for the presence of the B-tubule projections (present in doublets 5 and 6), no differences were present between these two group averages (data not shown). We then generated individual doublet averages for *bop2-1* doublets 5, 6, 8, and 9 and compared them to the overall grand average from all the wild-type outer doublets. Difference images are shown in Fig. 7 (*a–d*). *bop2-1* outer doublets 5, 6, and 8 are missing intensity in both lobes whereas *bop2-1* doublet 9 is missing intensity only from the lobe in the inner domain (compare Figs. 4 *c* and 7, *a–d*). We also generated a difference image between a group average of *bop2-1* outer doublets 5, 6, 8, and 9 and the overall wild-type outer doublet grand average (Fig. 7 *e*). This difference image is quite similar to the image obtained when the *bop2-1* grand average is compared to wild-type (compare Figs. 4 *c* and 7 *e*). Therefore, the *bop2-1* outer doublets with significantly less intensity in the inner arm region (Fig. 6) can be put into two classes with doublets 5, 6, and 8 missing more inner arm region density than doublet 9.

Even though the entire inner arm region intensities of doublets 2, 3, 4, and 7 from *bop2-1* axonemes are not significantly less than the intensities in the corresponding wild-type doublets (Fig. 6), we examined the structure of these doublets as a group. The inner arm region structure of *bop2-1* doublets 2, 3, 4, and 7 was compared to the wild-type grand average and a difference image is shown in Fig. 7 *f*. This difference image shows that doublets 2, 3, 4, and 7 exhibit a less severe deficiency in the inner arm region. It is likely that this less severe deficiency did not show up in the analysis shown in Fig. 6 because our first analysis compared the entire inner arm region intensity between *bop2-1* and wild-type axonemes and the second analysis compared the inner arm region structure pixel-by-pixel.

We also examined the structure of doublet 1 from wild-type and *bop2-1* strains to determine if the *bop2-1* mutation affects the morphology of doublet 1. The morphology of doublet 1 is clearly different from the structure of the other eight doublets (Mastronarde et al., 1992). Further complexity may exist in the biochemical composition of doublet 1 since

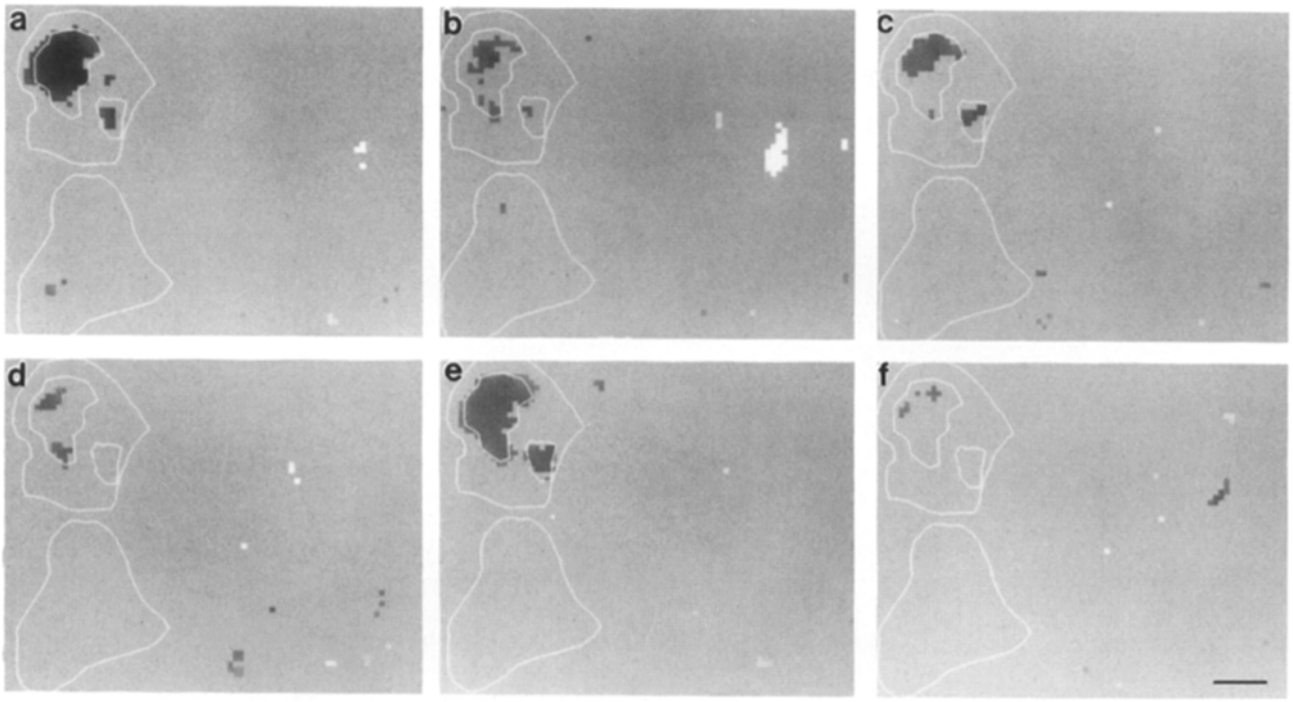

Figure 7. Difference images with various *bop2-1* averages. The outlines are the same as in Fig. 4 *c*. All *bop2-1* averages are compared to the wild-type grand average ($n = 268$). (*a*) The difference image with *bop2-1* doublet 5 ($n = 33$). (*b*) The difference image with *bop2-1* doublet 6 ($n = 40$). (*c*) The difference image with *bop2-1* doublet 8 ($n = 37$). (*d*) The difference image with *bop2-1* doublet 9 ($n = 41$). (*e*) The difference image with *bop2-1* doublets 5, 6, 8, and 9 ($n = 151$). (*f*) The difference image with *bop2-1* doublets 2, 3, 4, and 7 ($n = 150$). Differences not significant at the 0.05 level of confidence were set to zero. Bar, 10 nm.

two classes of doublet 1 morphology are present along the length of the doublet. We did not include the doublet 1 images that contained the two-membered cross-bridge in our analysis because of the large variability this would introduce. Cross-sectional images from wild-type and *bop2-1* axonemes were normalized on the microtubule doublet, rather than the outer dynein arm, and then compared as described previously. We constructed a difference image between wild-type doublet 1 ($n = 22$ images) and *bop2-1* doublet 1 ($n = 29$ images) averages. No differences were present between the two images ($p = 0.214$). Therefore, the *bop2-1* mutation does not affect the structure of the inner arm region of doublet 1.

Our analyses have identified three classes of *bop2-1* doublets. The class with the most severe phenotype is comprised of doublets 5, 6, and 8. Doublet 9 has an intermediate phenotype and doublets 2, 3, 4, and 7 have the least severe phenotype. Therefore, not only does the *bop2-1* mutation affect the assembly of inner arm region structures differently in specific doublets, but there are several different degrees of severity.

We examined the structural phenotype of *bop2-1* axonemes from proximal and distal/medial regions of the axoneme. 38% of the *bop2-1* images were from proximal regions of the axoneme as defined by the presence of either B-tubule projections or the two-membered cross-bridge. The proximal and the distal/medial regions of the axoneme contain equal percentages of affected outer doublets, and a comparison between the images of *bop2-1* doublets from these regions shows no differences ($p = 0.120$). Therefore, the structures affected in the *bop2-1* strain are not correlated to a known proximal/distal asymmetry.

Discussion

The Structural Phenotype of bop2-1 Axonemes

The *bop2-1* mutation affects the assembly of several structures in the inner dynein arm region and reveals a new asymmetry in the inner arm region. In cross-sectional images, doublets 5, 6, and 8 have the most severe phenotype, doublet 9 is intermediate, and doublets 2, 3, 4, and 7 have the least severe phenotype (Fig. 7). A subset of the density missing in doublets 5, 6, and 8 is missing in all the other doublets. We have attempted to correlate the radial asymmetry that we observe in cross-sectional images with the heterogeneity that we characterized in the individual longitudinal images (Fig. 8). Four inner arm region densities are missing in the most defective longitudinal images; these include two of the densities missing in *ida4* axonemes, a portion of the drc, and the projection (Fig. 5 *j*). These images are likely to be of doublets 5, 6, and 8, which have the most severe defect in the cross-sectional analysis (Fig. 8 *b*). The remainder of the longitudinal images are missing a portion of the drc and the projection (Fig. 5 *h*). We propose that these images are of doublets 2, 3, 4, and 7, which have a less severe defect (Fig. 8 *c*). Doublet 9 has an intermediate phenotype in the cross-sectional images and we do not see an intermediate phenotype among the longitudinal images. It is possible that we have not sampled doublet 9 among the 10 longitudinal im-

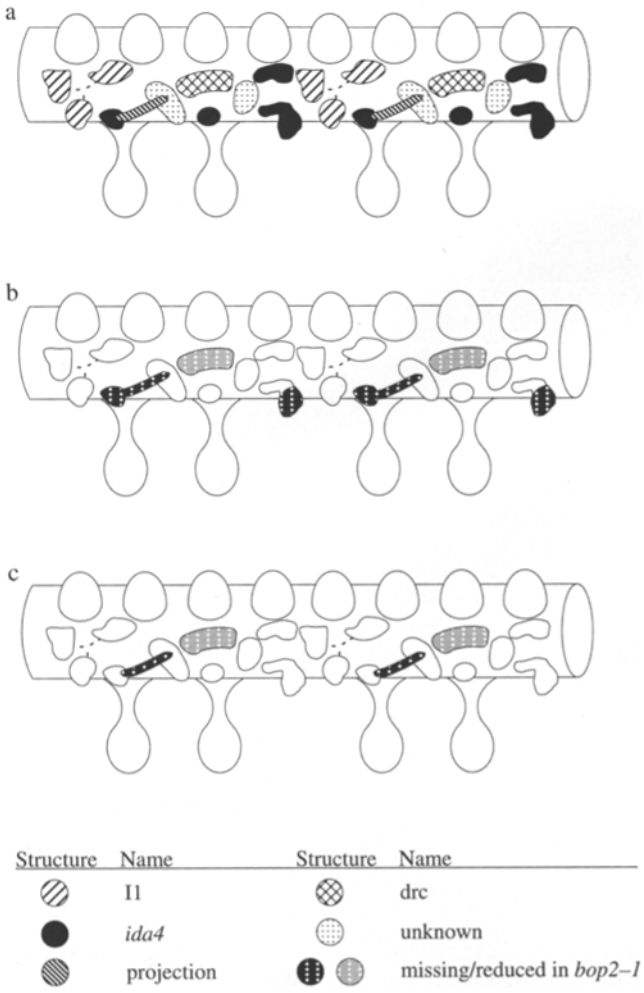

Figure 8. Model of structures along the A-subfiber of the outer doublet microtubule. Inner arm region structures are identified as described in Mastronarde et al. (1992) and this work. In *b* and *c* the black structures are missing and the gray structures are reduced in the appropriate *bop2-1* axonemes. (*a*) Model of structures in wild-type axonemes. (*b*) Model of structures missing from outer doublets, 5, 6, and 8 in *bop2-1* axonemes. (*c*) Model of structures missing from outer doublets, 2, 3, 4, and 7 in *bop2-1* axonemes.

ages examined ($p = 0.26$). Alternatively, the longitudinal image of doublet 9 may not be different enough from the images of doublets 2, 3, 4, and 7 to be detected in the longitudinal analysis of an individual axoneme. Our analyses are quite convincing that radial asymmetry alone accounts for the classes of cross-sectional and longitudinal morphologies.

The projection occupies an interesting position between a structure missing in *ida4* axonemes and an unidentified structure in the inner arm region that is likely to be a different dynein species. Kagami and Kamiya (1992) purified inner arm axonemal HMW dyneins into seven fractions that contain eight biochemically definable HMW dyneins. Mutational and structural analyses have shown that five of these HMW dyneins are likely to comprise that I1 and *ida4* inner dynein arms. The remaining three HMW dyneins are not missing in any known mutant strains; they are likely to be located in the two unidentified structures in the longitudinal view of the axoneme (Fig. 8 *a*). Thus the projection could play a role in the binding or regulation of dynein subspecies, transmitting signals between different dyneins, or be a part of a dynein.

Biochemical Analysis of bop2-1 Axonemes

Although four structures are missing or reduced in *bop2-1* axonemes, only a single polypeptide is completely missing. It is a phosphoprotein with an apparent molecular weight of 152,000 that is not missing in any of the previously described flagellar mutant strains. We did not observe the complete loss of any known *ida4* or drc polypeptides (Huang et al., 1982*b*; Kamiya et al., 1991; Piperno et al., 1992) but it is possible that these polypeptides are reduced. Based on the longitudinal image data, we have considered three potential locations for the 152-kD polypeptide; they are the *ida4* inner arms, the drc, and the projection. We consider the *ida4* inner arms and the drc to be unlikely locations as this polypeptide is not missing in axonemes from the *ida4*, *pf2*, or *pf3* strains. Further evidence against a drc location is that the 152-kD polypeptide is extractable by treatment with high salt (Inwood, 1985) whereas the components of the drc are not extractable by high salt (Piperno et al., 1981, 1992). Thus, it seems likely that the 152-kD polypeptide may be a component of the projection. Given the likely location and the extractability of the 152-kD polypeptide, it is possible that it could be part of one of the three uncharacterized dynein species (Kagami and Kamiya, 1992).

We have attempted to ask if the 152-kD polypeptide is the gene product of the *BOP2* locus using both dikaryon rescue analysis and reversion analysis. We failed to find any intragenic reversion events at the *BOP2* locus from the reversion analysis. The results of the dikaryon analysis are consistent with the 152-kD polypeptide being the gene product of the *BOP2* locus. However, an alternative explanation for the dikaryon analysis results is that the 152-kD polypeptide is not the gene product but is assembled into a complex in the cytoplasm that requires the Bop2 gene product for stability. Results from Luck and Piperno (1989) and Porter et al. (1992) on other dynein mutations support this second model. The identification of the gene product of the *BOP2* locus must await further genetic and molecular analyses.

Genetic Analysis of the bop2-1 Mutation

The *bop2-1* allele was identified as a suppressor of the nonswimming phenotype of the *pf10* mutation (Dutcher et al., 1988). Only one *bop2* allele was found among 70 independent extragenic suppressors of *pf10* and this allele was one of only 13 suppressor mutations that was able to suppress in the absence of light (Dutcher et al., 1988). We have screened a new collection of suppressors of the pf10 nonswimming phenotype that act in the absence of light. Among 73 newly isolated suppressed strains, we have failed to find any *bop2* alleles (Shirley, R. L., S. J. King and S. K. Dutcher, work in progress). This preliminary result suggests that the *bop2-1* allele is a highly unusual allele and that different alleles at this locus may have dramatically different phenotypes. Thus, it remains an important question to determine if the *bop2-1* allele makes a product with partial or altered activity or is a null allele and makes no product.

Role of Radial Asymmetry in Flagellar Motility

To use the asymmetric waveform it is necessary to activate

and inactivate the dynein arms in a specific pattern radially around the axoneme (Omoto and Kung, 1979; Fox and Sale, 1987). It is unlikely that this asymmetrical activation/inactivation is achieved simply through the outer dynein arms. Structural, biochemical and genetic analyses have suggested that the outer dynein arms are structurally equivalent and the waveform of *oda*⁻ mutant strains is not altered from that of wild-type axonemes (Piperno et al., 1981; Mitchell and Rosenbaum, 1985; Brokaw and Kamiya, 1987; Kamiya, 1988). However, the motile flagellar mutant strains with defects in the assembly of inner arm dyneins or in the dynein regulatory complex have waveforms that are more sinusoidal in appearance than the asymmetric waveforms of wild-type axonemes (Brokaw et al., 1982; Brokaw and Kamiya, 1987). A complete complement of structures in the inner arm region may be necessary for asymmetric waveforms. In wild-type axonemes this asymmetrical activation is likely to be imposed on the inner dynein arms at least in part by the interactions of the central pair microtubules and radial spokes. This statement is supported by three observations. First, in vitro reactivated axonemes with extruded central pair microtubules produce a symmetric waveform (Hosokawa and Miki-Noumura, 1987). Second, when paralyzed mutant strains that lack radial spokes are suppressed by mutations in the drc, they show a symmetric waveform (Brokaw et al., 1982; Brokaw and Kamiya, 1987). Finally, Smith and Sale (1992) have shown that the radial spokes modify the inner dynein arms; the in vitro activity of isolated inner dynein arms as monitored by rates of microtubule sliding is slower when inner arms are isolated from axonemes with mutant radial spokes compared to wild-type axonemes. Therefore, morphological and biochemical asymmetries in the inner dynein arms may provide one way to generate the characteristic asymmetric waveform. Given the biochemical complexity of the dyneins in the inner arms (Kagami and Kamiya, 1992), they are clearly a reasonable site for this type of control.

Four radial asymmetries have now been identified. These are the B-tubule projections, the two-membered cross-bridge, the absence of outer dynein arms, and the inner arm region structures described in this work. The two-membered cross-bridge and the B-tubule projections, because of their localization to the proximal portions of outer doublets and their location in the beat plane of the flagella, are ideal candidates for structures that are involved in the control of the planar power stroke with the correct spatial orientation. The absence of outer dynein arms from doublet 1, along with the two-membered cross-bridge, may act to prevent effective microtubule sliding between doublets 1 and 2 along the length of the axoneme. One possible role for radial asymmetry in the inner dynein arm region may be to allow certain subsets of arms to function as units in the generation of force (Sale, 1986; Lindemann et al., 1992).

Identification of radial asymmetries in both sea urchin and rat sperm flagella supports the hypothesis that different groups of outer doublets may function as a unit in the generation of force. Sea urchin and rat sperm flagella use the sinusoidal beat pattern exclusively, whereas this pattern is observed rarely in *Chlamydomonas* flagella. Two functional outer doublet groups have been identified in sea urchin sperm flagella; one group contains doublets 8, 9, 1, 2, 3, and the central pair whereas the other group contains doublets 4, 5, 6, and 7 (Sale, 1986). Three functional outer doublet groups have been identified in rat sperm flagella; the first group contains doublets 9, 1, and 2, a second group contains doublets 4, 5, 6, and 7, and the final group contains doublet 8, the central pair complex, and doublet 3 (Lindemann et al., 1992). In each of the sperm flagella, the organization of the functional groups is thought to promote microtubule sliding only in the plane of the sinusoidal beat. A second difference between the sperm flagella and *Chlamydomonas* flagella is that both sea urchin and rat sperm flagella contain central pair complexes that do not rotate. In contrast, *Chlamydomonas* flagella contain a central pair complex that rotates and is thought to regulate specific doublet dyneins in a spatial and temporal manner (Kamiya, 1982; Kamiya et al., 1982). A complex pattern of dynein activation and inactivation would be required to generate both a planar power stroke and a three-dimensional recovery stroke. Therefore, while the three classes of affected *bop2-1* doublets do not fit into a pattern as simple as those seen in the sperm flagella, outer doublets 5, 6, 8, and 9 may also be members of one or more functional outer doublet groups. The effect of the *bop2-1* mutation may be to disrupt the structure of a subset of outer doublet functional groups that are required to work in coordination in the complex *Chlamydomonas* flagellar beat pattern.

We thank A. E. McBride for help with the reversion analysis, D. N. Mastronarde for help with the image analysis, A. L. Palombella for help with the computer graphics, and P. Matsudaria and M. E. Porter for the orientation correction of the longitudinal analysis. We also thank L. L. Ehler, A. L. Palombella, and J. R. McIntosh for helpful criticisms of this manuscript.

This work was supported by grants from the National Institutes of Health (GM-32843) to S. K. Dutcher and (RR-00592) to J. R. McIntosh and in part by an award to S. K. Dutcher from the Searle Scholar's Program. W. B. Inwood and S. J. King were supported in part by traineeships from NIH (5T32-GM-07135).

Received for publication 30 March 1994 and in revised form 6 June 1994.

Note Added in Proof. With the characterization of the *ida5* and *ida6* strains, only two of the eight biochemically defined HMW dyneins remain unidentified by mutational analyses.

References

Adams, G. M. W., B. Huang, G. Piperno, and D. J. L. Luck. 1981. Central-pair microtubular complex of *Chlamydomonas* flagella: polypeptide composition as revealed by analysis of mutants. *J. Cell Biol.* 91:69–76.

Blum, H., H. Beier, and H. J. Gross. 1987. Improved silver staining of plant proteins, RNA and DNA in polyacrylamide gels. *Electrophoresis.* 8:93–97.

Brokaw, C. J., and R. Kamiya. 1987. Bending patterns of *Chlamydomonas* flagella: IV. Mutants with defects in inner and outer dynein arms indicate differences in dynein arm function. *Cell Motil.* 8:68–75.

Brokaw, C. J., D. J. L. Luck, and B. Huang. 1982. Analysis of the movement of *Chlamydomonas* flagella: the function of the radial-spoke system is revealed by comparison of wild-type and mutant flagella. *J. Cell Biol.* 92:722–732.

Dentler, W. L., and C. Adams. 1992. Flagellar microtubule dynamics in *Chlamydomonas*: cytochalasin D induces periods of microtubule shortening and elongation; and colchicine induces disassembly of the distal, but not proximal, half of the flagellum. *J. Cell Biol.* 117:1289–1298.

Dutcher, S. K. 1986. Genetic properties of linkage group XIX in *Chlamydomonas reinhardtii*. *In* Extrachromosomal Elements in Lower Eukaryotes. R. B. Wickner, A. Hinnebusch, A. M. Lambowitz, I. C. Gunsalus, and A. Hollaender, editors. Plenum Publishing Corp., New York. 303–325.

Dutcher, S. K., W. Gibbons, and W. B. Inwood. 1988. A genetic analysis of suppressors of the *PF10* mutation in *Chlamydomonas reinhardtii*. *Genetics.* 120:965–976.

Dutcher, S. K., B. Huang, and D. J. L. Luck. 1984. Genetic dissection of the central pair microtubules of the flagella of *Chlamydomonas reinhardtii*. *J. Cell Biol.* 98:229–236.

Fox, L. A., and W. S. Sale. 1987. Direction of force generated by the inner row of dynein arms on flagellar microtubules. *J. Cell Biol.* 105:1781–1787.

Harris, E. H. 1989. The *Chlamydomonas* Sourcebook. Academic Press, San Diego. 780 pp.

Holmes, J. A., and S. K. Dutcher. 1989. Cellular asymmetry in *Chlamydomonas reinhardtii*. *J. Cell Sci.* 94:273–285.

Hoops, H. J., and G. B. Witman. 1983. Outer doublet heterogeneity reveals structural polarity related to beat direction in *Chlamydomonas* flagella. *J. Cell Biol.* 97:902–908.

Hosokawa, Y., and T. Miki-Noumura. 1987. Bending motion of *Chlamydomonas* axonemes after extrusion of central-pair microtubules. *J. Cell Biol.* 105:1297–1301.

Huang, B., G. Piperno, and D. J. L. Luck. 1979. Paralyzed flagella mutants of *Chlamydomonas reinhardtii* defective for axonemal doublet microtubule arms. *J. Biol. Chem.* 254:3091–3099.

Huang, B., G. Piperno, Z. Ramanis, and D. J. L. Luck. 1981. Radial spokes of *Chlamydomonas* flagella: genetic analysis of assembly and function. *J. Cell Biol.* 88:80–88.

Huang, B., Z. Ramanis, S. K. Dutcher, and D. J. L. Luck. 1982*a*. Uniflagellar mutants of *Chlamydomonas*: evidence for the role of basal bodies in transmission of positional information. *Cell.* 29:745–753.

Huang, B., Z. Ramanis, and D. J. L. Luck. 1982*b*. Suppressor mutations in *Chlamydomonas* reveal a regulatory mechanism of flagellar function. *Cell.* 28:115–124.

Inwood, W. B. 1985. A reversion analysis of an abnormal swimming mutation in *Chlamydomonas reinhardtii*. Ph.D. thesis, University of Colorado at Boulder, Boulder, CO. 156 pp.

Kagami O., and R. Kamiya. 1992. Translocation and rotation of microtubules caused by multiple species of *Chlamydomonas* inner-arm dynein. *J. Cell Sci.* 103:653–664.

Kamiya, R. 1982. Extrusion and rotation of the central-pair microtubules in detergent-treated *Chlamydomonas* flagella. *Cell Motil.* 1(Suppl):169–173.

Kamiya, R. 1988. Mutations at twelve independent loci result in absence of outer dynein arms in *Chlamydomonas reinhardtii*. *J. Cell Biol.* 107:2253–2258.

Kamiya, R., E. Kurimoto, and E. Muto. 1991. Two types of *Chlamydomonas* flagellar mutants missing different components of inner-arm dynein. *J. Cell Biol.* 112:441–447.

Kamiya, R., R. Nagai, and S. Nakamura. 1982. Rotation of the central-pair microtubules in *Chlamydomonas* flagella. *In* Biological Functions of Microtubules and Related Structures. H. Sakai, H. Moiri, and G. G. Borisy, editors. Academic Press, Inc., New York. 189–198.

Kamiya, R., and G. B. Witman. 1984. Submicromolar levels of calcium control the balance of beating between the two flagella in demembranated models of *Chlamydomonas*. *J. Cell Biol.* 98:97–107.

Kato, T., O. Kagami, T. Yagi, and R. Kamiya. 1993. Isolation of two species of *Chlamydomonas reinhardtii* flagellar mutants, *ida5* and *ida6*, that lack a newly identified heavy chain of the inner dynein arm. *Cell Struct. Funct.* 18:371–377.

Levine, R. P., and W. Ebersold. 1960. The genetics and cytology of *Chlamydomonas*. *Annu. Rev. Microbiol.* 14:197–216.

Lindemann, C. B., A. Orlando, and K. S. Kanous. 1992. The flagellar beat of rat sperm flagella is organized by the interaction of two functionally distinct populations of dynein bridges with a stable central axonemal partition. *J. Cell Sci.* 102:249–260.

Luck, D. J. L., and G. Piperno. 1989. Dynein arm mutants in *Chlamydomonas*. *In* Cell Movement. F. D. Warner, P. Satir, and I. R. Gibbons, editors. Alan R. Liss Inc., New York. 49–60.

Luck, D. J. L., G. Piperno, Z. Ramanis, and B. Huang. 1977. Flagellar mutants of *Chlamydomonas*: studies of radial spoke-defective strains by dikaryon and revertant analysis. *Proc. Natl. Acad. Sci. USA.* 74:3456–3460.

Lux III, F. G., and S. K. Dutcher. 1991. Genetic interactions at the *FLA10* locus: suppressors and synthetic phenotypes that affect the cell cycle and flagellar function in *Chlamydomonas reinhardtii*. *Genetics.* 128:549–561.

McVittie, A. 1972. Flagellum mutants of *Chlamydomonas reinhardtii*. *J. Gen. Microbiol.* 71:525–540.

Mastronarde, D. N., E. T. O'Toole, K. L. McDonald, J. R. McIntosh, and M. E. Porter. 1992. Arrangement of inner dynein arms in wild-type and mutant flagella of *Chlamydomonas*. *J. Cell Biol.* 118:1145–1162.

Merrill, C. R., D. Goldman, S. A. Sedman, and M. H. Ebert. 1981. Ultrasensitive stain for proteins in polyacrylamide gels shows variation in cerebrospinal fluid proteins. *Science (Wash. DC).* 211:1437–1439.

Mitchell, D. R., and Y. Kang. 1993. Reversion analysis of dynein intermediate chain function. *J. Cell Sci.* 105:1069–1078.

Mitchell, D. R., and J. L. Rosenbaum. 1985. A motile *Chlamydomonas* flagellar mutant that lacks outer dynein arms. *J. Cell Biol.* 100:1228–1234.

Muto, E., R. Kamiya, and S. Tsukita. 1991. Double-rowed organization of inner dynein arms in *Chlamydomonas* flagella revealed by tilt-series thin-section electron microscopy. *J. Cell Sci.* 99:57–66.

Omoto, C. K., and C. Kung. 1979. The pair of central tubules rotates during ciliary beat in *Paramecium*. *Nature (Lond.).* 279:532–534.

Piperno, G., B. Huang, Z. Ramanis, and D. J. L. Luck. 1981. Radial spokes of *Chlamydomonas* flagella: polypeptide composition and phosphorylation of stalk components. *J. Cell Biol.* 88:73–79.

Piperno, G., K. Mead, and W. Shestak. 1992. The inner dynein arms I2 interact with a "dynein regulatory complex" in *Chlamydomonas* flagella. *J. Cell Biol.* 118:1455–1463.

Piperno, G., and Z. Ramanis. 1991. The proximal portion of *Chlamydomonas* flagella contains a distinct set of inner dynein arms. *J. Cell Biol.* 112:701–709.

Piperno, G., Z. Ramanis, E. F. Smith, and W. S. Sale. 1990. Three distinct inner dynein arms in *Chlamydomonas* flagella. Molecular composition and location in the axoneme. *J. Cell Biol.* 110:379–389.

Porter, M. E., J. Power, and S. K. Dutcher. 1992. Extragenic suppressors of paralyzed flagellar mutations in *Chlamydomonas reinhardtii* identify loci that alter the inner dynein arms. *J. Cell Biol.* 118:1163–1176.

Rüffer, U., and W. Nultsch. 1991. Flagellar photoresponses of *Chlamydomonas* cells held on micropipettes: II. Change in flagellar beat pattern. *Cell Motil.* 18:269–278.

Sale, W. S. 1986. The axonemal axis and Ca^{2+}-induced asymmetry of active microtubule sliding in sea urchin sperm tails. *J. Cell Biol.* 102:2042–2052.

Segal, R. A., B. Huang, Z. Ramanis, and D. J. L. Luck. 1984. Mutant strains of *Chlamydomonas reinhardtii* that move backwards only. *J. Cell Biol.* 98:2026–2034.

Smith, E. F., and W. S. Sale. 1992. Regulation of dynein-driven microtubule sliding by the radial spokes in flagella. *Science (Wash. DC).* 257:1557–1559.

Williams, D. W., M. A. Velleca, A. M. Curry, and J. L. Rosenbaum. 1989. Molecular cloning and sequence analysis of the *Chlamydomonas* gene coding for radial spoke protein 3: flagellar mutation *pf-14* is an ochre allele. *J. Cell Biol.* 109:235–245.